Received October 19, 2020, accepted November 8, 2020, date of publication November 17, 2020, date of current version December 1, 2020.

Digital Object Identifier 10.1109/ACCESS.2020.3038477

An Enhanced Lithium-Ion Battery Model for Estimating the State of Charge and Degraded Capacity Using an Optimized Extended Kalman Filter

RASOOL M. IMRAN[1], QIANG LI[1], AND FIRAS M. F. FLAIH[2], (Member, IEEE)
[1]School of Artificial Intelligence, Wuchang University of Technology, Wuhan 430223, China
[2]State Company of the North Distribution Electricity, Ministry of Electricity, Baghdad 10013, Iraq
Corresponding author: Rasool M. Imran (120160526@wut.edu.cn)

ABSTRACT Lithium-ion batteries have become the most appropriate batteries to use in modern electric vehicles due to their high-power density, long lifecycle, and low self-discharge rate. The precise estimation of the state of charge (SOC) in lithium-ion batteries is essential to assure their safe use, increase the battery lifespan, and achieve better management. Various methods of SOC estimation for lithium-ion batteries have been used. Among these methods, the model-based estimation method is the most practical and reliable. The accuracy of the utilized model is a crucial factor in realizing better SOC estimation in the model-based method. In this paper, an enhanced battery model is proposed to estimate the SOC precisely via an optimized extended Kalman filter. The model considers the most influencing factors on the estimation accuracy, such as temperature, aging, and self-discharge. The parameterization of the model has defined the dependency of sensitive parameters on state estimation. As a fundamental step before estimating the SOC, the capacity degradation is evaluated using a straightforward approach. Later, a particle swarm optimization algorithm is utilized to optimize the vector of process noise covariance to enhance the state estimation. The performance of the proposed method is compared to recent techniques in the literature. The results indicate the effectiveness of the proposed approach in terms of both accuracy and computational simplicity.

INDEX TERMS Lithium-ion battery, state of charge, capacity estimation, extended Kalman filter, PSO algorithm.

I. INTRODUCTION

Batteries are the best energy storage systems for various essential applications such as smartphones, computers, electric vehicles (EVs), power system enhancements, medical applications, drones, and satellites. Batteries are diverse in characteristics and prices according to their applications. The most common rechargeable batteries are lead-acid, lithium-ion, and metal-nickel-hydride. Recently, lithium-ion batteries have become the preferred choice in modern EVs due to their high power density, long lifecycle, broad temperature operating range, fast charging ability, and low self-discharge [1]. Accordingly, a significant factor in improving EV performance is handling the management and estimation issues for the essential states of lithium-ion batteries. Estimating the state of charge (SOC) in lithium-ion batteries is a crucial issue to satisfy safe use and better battery management.

Numerous approaches have been used to estimate the SOC of lithium-ion batteries. The direct open-circuit voltage (OCV) based method is straightforward and cost-effective. This approach works by assigning an SOC value for each value of the battery output voltage in the open-circuit state [2]–[4]. The most appropriate manner of applying the OCV method is by using a 2D lookup table of SOC and OCV values [5]. Generally, the OCV-based method requires a few simple components to be implemented. However, obtaining an accurate OCV when the battery is under operation is not achievable for most batteries. Lithium-ion batteries need long relaxation time to obtain an accurate OCV after disconnecting the battery. Additionally, the OCV-based method is

The associate editor coordinating the review of this manuscript and approving it for publication was Seyedali Mirjalili.

profoundly affected by the aging process of the battery [6]. The current integrating (Coulomb counting) method can be used to calculate the descent or growth of an SOC based on the energy transferred from or to the battery [7], [8]. This method works efficiently for online SOC estimation. However, estimation errors can occur due to measurement noise and battery self-discharging, especially during a long battery rest [9]. Furthermore, this approach requires knowing both the initial SOC at each operation and the state of health (SOH) to update the current capacity of the battery [10]. Estimating the SOC based on measuring the chemical impedance by means of applying an AC current through the battery at different frequencies is an efficient method that is more precise than both previous methods [11], [12]. However, this method is not universal and not easily used in online applications. Intelligent algorithm-based SOC estimation methods (*i.e.*, artificial neural networks ANNs and neuro-fuzzy networks) have been proposed in [13]–[15]. These methods require intensive training offline to be appropriately used online. Indirect model comparison-based methods are considered the most practical methods to estimate an accurate SOC. These methods calculate and mitigate the error of SOC estimation by comparing the output parameters of the original battery to a designed battery model via a PI controller, Lagrange multiplier, or Kalman filter configuration [16]–[18]. The method complexity and the difficulty of obtaining a realistic model for the battery are two vulnerabilities of this method. Hence, finding a precise and straightforward model is a vital issue that demands the model-based method be utilized for estimating the SOC broadly [19]–[23]. A recent trend to estimate the correct SOC that utilizes the hybrid combination of two or more of the previous estimation methods was proposed in [6], [24]. This trend ensures high accuracy at different operating conditions; however, some restrictions arise in the use of this method, such as low reliability and high processing burden due to the simultaneous use of multiple estimation techniques [25]. In general, three main aspects must be considered to improve the SOC estimation of lithium-ion batteries, the precision of current and voltage sensors, the reality of the battery model to match the original battery under different operating conditions, and the accuracy of capacity estimation. Estimating the capacity is a fundamental step for the dynamic process of accurate SOC assessment. Additionally, knowing the degraded capacity aids in defining the SOH of the battery. The differential capacity rate (dQ/dV) has been used for detecting the aging process and assessing the degraded capacity in [26]–[28]. As this rate changes with the energy capability of the battery for a specific SOC range, this approach is considered one of the most effective techniques for capacity estimation. Such an approach uses curve fitting and regression techniques to define the peak of the dQ/dV curve, which is used to assess the current capacity. A shortcoming of this method is related to the need for the dQ/dV curve of the used battery, which may be attained via a supplemental and time-consuming analytical process such as cyclic voltammetry. Other studies have used the direct Coulomb counting method to estimate the capacity degradation with the aid of a Kalman filter, forming a model-based estimating structure [29], [30]. First, the capacity is measured by integrating the discharging current for a specific period due to the corresponding change in SOC (ΔSOC). Second, a Kalman filter is applied to extract the measurement noise and track the actual capacity. Regardless of increasing the complexity by adding an extra Kalman filter, these methods necessitate the availability of the correct ΔSOC or at least a ΔSOC with a tiny error that can be minimized due to the closed loop of two observers because the SOC itself relays primarily on the estimated capacity. Another approach has utilized the direct Coulomb counting technique supported by the recursive total least square (RTLS) method to calculate the battery capacity [31], [32]. This approach requires interaction with an algorithm to detect the capacity loss (*e.g.*, observing the charging-time shortness).

To this end, we believe that the mentioned methods for estimating both the SOC and capacity of lithium-ion batteries have involved a tradeoff between the estimation accuracy and complexities of both design and computation. This paper aims to address two of the aforementioned aspects to enhance the SOC estimation for the lithium-ion batteries potentially used in EVs, namely, the battery model precision and capacity estimation accuracy. A precise lithium-ion battery model is developed that considered the effects of operating temperature, aging process, and self-discharge. The model takes into account the research gaps in the literature to enhance the estimation accuracy with avoiding design complexity and reducing the computational burden. The proposed model is supported by a new approach to estimate the capacity degradation that utilizes, in a closed-loop manner, both voltage decay and measured capacity via Columb counting. Later, a sensitivity analysis is conducted to determine which parameters of the proposed model have severe impacts on state estimation. The proposed model and capacity estimation can be used with different state observers (*e.g.*, any of Kalman filters family or particle filter (PF)) to estimate the SOC accurately. However, the extended Kalman filter (EKF) is chosen among other types of filters because it deals effectively with slightly nonlinear systems compared to the basic Kalman filter. Additionally, the EKF obtains a better match to this problem compared to the PF and other types of nonlinear Kalman filters in considering both computational cost and simplicity aspects, as will be outlined in Section III. Two adjustable parameters affect the estimation performance of EKF; the measurement noise covariance (R) and the process noise covariance (Q). R can be set by attaining multiple measures from the sensor due to a constant input and then discounting the mean value so that the noise covariance can be acquired. Q can be set intuitively or by the trial and error method, which is tedious and inaccurate; this can lead to filtering divergence over a long operating time, especially when R is set relatively small [33]. Thus, several optimization algorithms are applied to attain the optimal vector of Q that ensures precise estimation, such as the genetic algorithm (GA) [34], differential evolution (DE) [35], and biogeography-based optimization (BBO) [36]. However, none was applied to tune observers for battery states estimation. In this paper, particle swarm optimization (PSO) is used to optimize the Q vector and enhance the performance of the EKF because it is considered faster in convergence and relatively simple [37]. PSO is applied to determine the optimal Q through a fitness function that reduces the estimation error covariance (P) of the EKF. Finally, the effectiveness of the proposed approach is verified via simulation results in the MATLAB/Simulink environment. Taking into account the mentioned points, the main contributions of this paper are as follows:

1) Propose an enhanced lithium-ion battery model to estimate the SOC that addresses the effects of operating temperature, aging process, and self-discharge.
2) Introduce a new and straightforward approach to estimate the degraded capacity of the battery, which supports the SOC estimation.
3) Present a modification in the use of the extended Kalman filter by exploiting PSO to optimize the vector of process noise covariance.
4) Conduct a sensitivity analysis to assign the sensitive model parameters that need to be tuned carefully to ensure model accuracy.

The remaining of the paper has organized as follows: Section II describes the standard lithium-ion battery models along with detailing the proposed model. In Section III, the use of the EKF to estimate the SOC of lithium-ion batteries is presented along with clarifying the reason to consider the EKF a preferred choice for this problem. This section also comprises the optimization of the process noise covariance via PSO to support the precise SOC estimation. Section IV presents both the parameterization process to set the optimal model parameters and the sensitivity analysis to assign the sensitive parameters and their influence on state estimation. Section V covers case study scenarios, their results, study limitations, and performance discussion that involves the accuracy and computational complexity. Whereas the proposed work has concluded in Section VI.

II. ENHANCED BATTERY MODEL

A. MODEL STRUCTURE

Researchers have proposed and employed several models for lithium-ion batteries that emulate the operational behavior. In general, the models fall into two types; the first uses the electrochemical characteristics of the lithium-ion cell [9], [38].

This type uses equations to describe the electrochemical reactions in lithium-ion batteries, such as intercalations, diffusions, and migrations. The application complexity, the necessity for specialized experience in chemistry, and the need for particular modeling for each type of lithium-ion battery make utilizing this model inconvenient. The second type is equivalent circuit-based modeling. Table 1 shows the most common equivalent circuit models for SOC estimation and battery management systems (BMSs). The use of

TABLE 1. Types of Lithium-ion battery equivalent circuit-based models.

Model name	Model diagram	References
Basic RC model	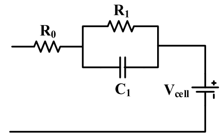	[6, 16, 22]
2 RC ladder model	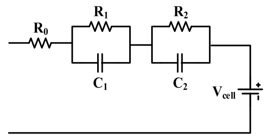	[18, 39-41]
Capacitor-based cell model	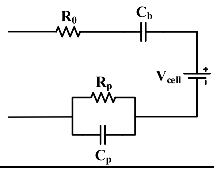	[19, 23]

voltage sources in all presented models is associated with the open-circuit potential. The series resistor is used to mimic the internal electrochemical resistivity and ionic conductivity of the battery, whereas the parallel set of resistor and capacitor is used to emulate the hysteresis effect or the delayed response of the OCV in both charging and discharging modes. Nevertheless, increasing the number of parallel capacitors will raise the computational challenge and increase the number of tuned parameters. Therefore, the basic resistance-capacitance (RC) model is used as the elementary model in this paper. The parameterization of the proposed RC model will be described in Section IV. The SOC can be formulated by its conventional definition as [19]:

$$SOC = SOC_0 - \frac{\int idt}{Q_{act}} \tag{1}$$

where SOC_0, Q_{act}, and i are the initial value of the SOC, the actual capacity of the battery, and the current of the battery, which is positive in the discharging mode and negative in the charging mode. The potential difference between the terminals of RC components in the proposed RC model can be clarified as:

$$V_C = \left(i - C\frac{dV_C}{dt}\right)R_1 \tag{2}$$

The dynamic equations of the battery model can be defined as:

$$\dot{V}_C = \frac{1}{C}I - \frac{1}{R_1 C}V_C \tag{3}$$

$$\dot{SOC} = -\frac{1}{3600Q_{act}}I \tag{4}$$

$$V_t = V_{OC} - V_C - R_{int}I \tag{5}$$

The temperature influence is added to the battery model, as shown in Fig. 1-b. The thermal model in Fig. 1-b refers to a heat exchange block that generates the temperature supposed

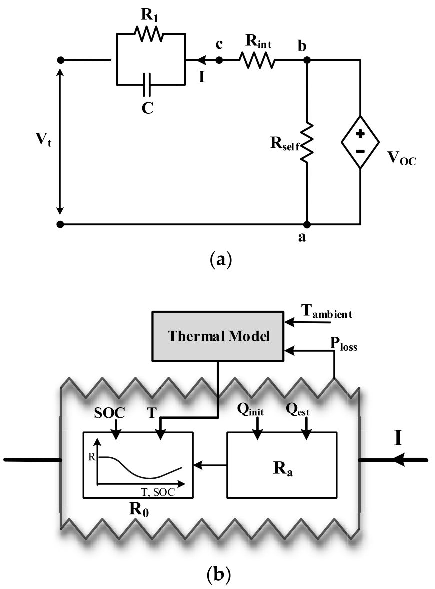

FIGURE 1. Lithium-ion battery: (a) Proposed battery model, (b) Proposed internal resistance model.

to achieve from the thermal sensor, which relies primarily on ambient temperature ($T_{ambient}$) and wasted power in the internal resistance (P_{loss}), where $P_{loss} = R_{int}I^2$. The output temperature (T) can be given by solving the heat equilibrium equation [42]:

$$C_P \frac{dT}{dt} = P_{loss} - \frac{T - T_{ambient}}{R_T} \tag{6}$$

where C_P and R_T are the specific heat capacity and thermal resistance, respectively. Taking the Laplace transform for (6) gives

$$T = \frac{R_T P_{loss} + T_{ambient}}{1 + C_P R_T s} \tag{7}$$

The self-discharge is mainly dependent on the off-period during the rest time and the internal temperature. Thus, the self-discharge is considered by means of inserting a large resistor (R_{self}) in parallel with the battery cell, and thus a minimal current will pass through it at the resting stage.

The proposed model thus considers the aging effect of the lithium-ion battery. Different reasons lie behind the aging process, such as the active mass loss, cyclable lithium consumption, and size increment of the surface layer. All these reasons contribute in one way or another to the proportional growth of electrochemical resistance [31]. Thus, to compile the aging effect, a slight increment in the internal resistance needs to be added correspondingly. This increment is determined based on the difference between the manufacturing capacity and the estimated capacity at each operating cycle. Therefore, a simple loop of a proportional controller is added to the initial internal resistance with a relatively small proportional gain (R_a) as:

$$R_{int} = R_0 + R_a(Q_{init} - Q_{est}) \tag{8}$$

where Q_{init}, Q_{est}, and R_0 are the manufacturing capacity, the estimated capacity, and the initial internal resistance of the battery, respectively. R_0 is built as a function of the battery temperature and SOC and formed via a lookup table. R_a can be tuned when other variables in (8) are known for particular temperatures and SOCs. For specific temperature and SOC, the actual R_{int} is considered the ohmic internal resistance of the battery, which can be measured via the AC current injection method.

B. DEGRADED CAPACITY MODEL

Currently, there are several methods used to recharge lithium-ion batteries. Among these methods, constant current–constant voltage (CCCV) and multistage constant current (MSCC) are the most common, and they are considered references for further modifications [43]. Fig. 2 describes the typical voltage-current profiles of both methods. In this work, the MSCC method is employed because it requires a shorter charging time, and it can reach full capacity even at low temperatures [1]. In MSCC charging, a large constant current (*e.g.*, 1 C-rate) is applied at the beginning to charge more than half of the capacity. When the voltage reaches a maximum limit, the constant current moves to a lower level according to the number of stages. Each stage ends when the voltage reaches the same maximum limit to avoid cell damage. In general, considering both the MSCC and CCCV methods, the charging current decreases gradually when the battery is nearly fully charged. At the same time, the maximum voltage of the battery for the current cycle can be attained.

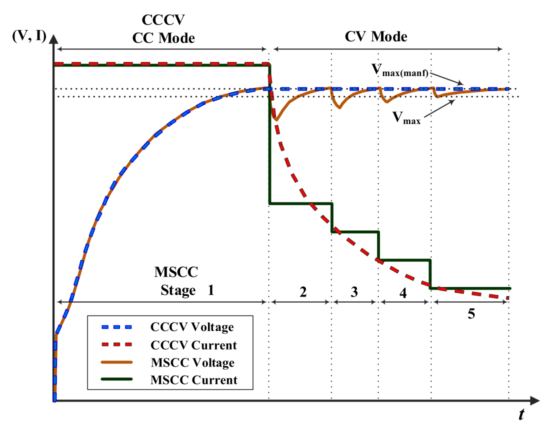

FIGURE 2. Voltage-current profiles during the charging mode of Lithium-ion batteries.

The basic concept of modeling the current capacity in this paper is straightforward as it relies on the available information from the charging mode at each cycle. Given that a slight decay in the battery maximum voltage (V_{max}) occurs during the natural degradation of capacity due to the increment in internal resistance, which results in reducing the power density [44]. Therefore, if V_{max} can be measured accurately at the end of the charging mode, the rate of degradation in the capacity can be modeled. Taking into account five stages of MSCC with currents of 1, 0.5, 0.4, 0.3, and 0.2 of the nominal charging current (I_{nom}), respectively. At the beginning of stage 5, when the charging current becomes 0.2 of I_{nom}, V_{max} can be measured (see Fig. 2). At stage 5, dV/dt is the smallest, and even if it is not zero, the voltage growth at this stage is temporary due to the charging current, and it will fade when the charging current is cut off at the full charge. The acquired V_{max} in stage 5, after noise extraction via a low-pass filter (LPF), is considered as the current V_{max} of the particular cycle. The modeled degraded capacity (Q_{model}) of the battery can be defined as a function of the current V_{max} at each cycle in (9). To ensure that the modeled capacity is converging to the actual capacity, a recalibration is needed based on the measured capacity by charging-current integration in stage 4. The measured capacity between the beginning SOC (SOC_b) and ending SOC (SOC_e) at stage 4 is defined in (11). Eventually, both modeled and measured capacities participate in estimating the current capacity of the battery via a PI-based closed-loop compensator, as given in (12). Because a very slight capacity loss occurs during each cycle, when the charging process ends before stage 5, V_{max} can be considered the same as the previous cycle.

$$Q_{model} = Q_{init}\left(V_m / V_{max(manf)}\right) \tag{9}$$

$$V_m = \frac{\omega_c}{\omega_c + s} V_{max} \tag{10}$$

$$Q_{meas} = \frac{I}{s(SOC_e - SOC_b)} \tag{11}$$

$$Q_{est} = Q_{model} + \left(K_p + \frac{K_i}{s}\right)(Q_{model} - Q_{meas}) \tag{12}$$

where $V_{max(manf)}$, V_m, ω_c, K_p, and K_i are the manufacturing value of the maximum battery voltage, the maximum voltage of the current cycle after passing through an LPF, the cutoff frequency of LPF (*i.e.*, 10 rad/s), the PI proportional gain (*i.e.*, 0.43×10^{-3}), and the PI integral gain (*i.e.*, 0.08×10^{-3}), respectively.

Note that the PI proportional and integral gains are tuned via the trial and error method with several iterations since the capacity convergence can be easily observed during gains tuning. The newly estimated capacity will be set during the transition between charging and discharging modes. A schematic diagram to clarify the procedure of capacity estimation is depicted in Fig. 3. The estimated capacity will be used to determine R_{int} and replace Q_{act} in (1) in order to estimate the SOC. The suggested battery model ensures that the internal resistance, terminal voltage, and capacity will be influenced in accordance with temperature change, which emulates battery performance under a real-world scenario.

III. IMPLEMENTING THE OPTIMIZED EXTENDED KALMAN FILTER

Fig. 4 clarifies the typical structure for SOC estimation in model-based methods. In general, all model-based methods are feedback-based state observers where the SOC represents the deduced state of the system based on the available knowledge of measurements and the known dynamics of the system. One of the suggested observers for this issue is the PI observer, which is applied in [20], [21]. Regardless of the simplicity of PI structure and the low cost of implementation, the PI observer estimates the state of a linear system. For a nonlinear system, an additional technique may need to be implemented to decompose the nonlinear system to several linear subsystems, and that may require adaptive PI gains. Given that the battery model has some randomness, including the process and measurement noises, the system state of the battery can be considered stochastic. A Kalman filter is primarily designed for stochastic systems, and thus it is more applicable for such estimation issues [45], [46]. However, the basic Kalman filter assumes a Gaussian distribution that should come from a linear function. In a lithium-ion battery, the relation between the output terminal voltage and the SOC is nonlinear, and thus the distribution may not be Gaussian. In this case, the basic Kalman filter may not appropriately estimate the system state. Development in the application of the linear Kalman filter has been proposed by locally linearizing the battery model using a piecewise linearization method [17], [18]. This approach necessitates the number of breaking intervals for piecewise linearization to be small in

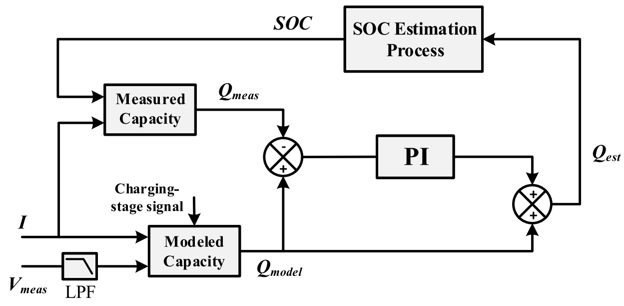

FIGURE 3. Schematic diagram of the capacity estimation procedure.

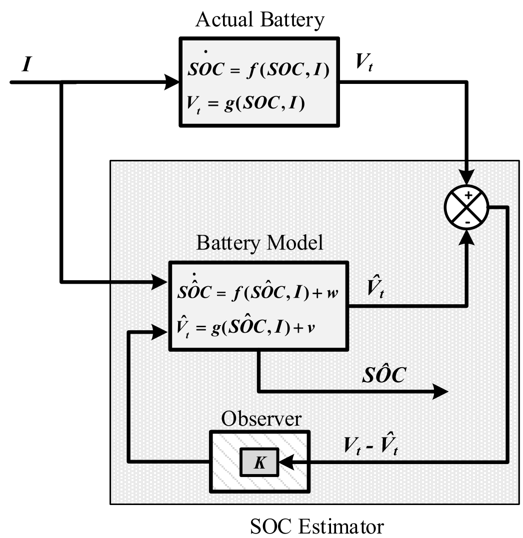

FIGURE 4. Typical structure for model-based SOC estimation approach.

order to avoid a heavy computational burden. As a result, with a minor error in the initial state, the combination of locally linearized Kalman filter (LLKF) works perfectly. Considering a significant error in the initial state, the LLKF takes a longer time to minimize the error and reach the actual state estimate, which will be proved in the Results section. The EKF and unscented Kalman filter (UKF) are the developed versions of the Kalman filter, these can be used for nonlinear systems [22], [23], [39]. The UKF creates a new distribution for the nonlinear function based on weighted points called sigma points (σ). The new sigma points form a new mean that makes a new Gaussian distribution. The main drawback of using the UKF is the need to accurately propagate a large number of sigma points with their weights, which is a costly procedure. In contrast, the advantages of the EKF are the relative ease of implementation and low computational cost. Both filters are implemented on embedded systems with limited computational resources. For many systems, the Jacobian matrix can be easily derived analytically, which makes the EKF implementation straightforward. Another area of potential advantage is the relative ease of tuning. The UKF has at least three tuning parameters: a sigma point spread, measurement noise, and process noise. Whereas the EKF has only two tuning parameters (measurement noise and process noise), these are well known from the universal Kalman filter.

The PF has been less used in SOC estimation until recently. A PF is primarily designed for nonlinear systems and non-Gaussian noise distribution [47]. A PF is a Monte Carlo-based estimation algorithm that uses a set of weighted particles (samples) to assess the posterior distributions of a stochastic-system state. Estimation via a PF includes four steps: initializing random particles, sampling the particles according to the new observations, resampling the particles based on assigned weight (negligible weight particles are replaced by higher weight particles), and normalization of weights to unity. A PF has four tuned parameters, namely, the number of particles, the initial particle location, the measurement noise covariance, and possibly process noise covariance. A PF offers the highest accuracy and fastest response (state update) when there are large initial state errors. However, with a correct initial state when the estimated state totally converges to the actual state, the accuracy of a PF is same or even lower than both the EKF and UKF, especially in the range of SOC when SOC-V_{OC} curve is almost flat because the weight of all samples is almost the same [48]. In terms of processing complexity, a PF is more complex than a UKF and requires a high-performance microcontroller to be applied because the Monte Carlo method employs a large number of weighted samples to form the distribution. Considering the above comparisons and given that the nonlinearity of SOC-V_{SOC} relationship is slight, the use of the EKF is the perfect choice for this state estimation issue because it works perfectly for quasilinear (slight nonlinear) systems [49]. Table 2 shows a comparison between the aforementioned model-based methods of SOC estimation, which is reached according to the above discussion and previous reviews [9].

TABLE 2. Common model-based observing methods for SOC.

Observing method	Reference	Processing complexity	Estimate accuracy	Response time	Parameter tuning complexity
PI/ Luenberger	[20, 21]	V. Low	Low	Low	V. Low
Linear KF	[45, 46]	Low	Low	Low	Low
LLKF	[17, 18]	Medium	Medium	Low	Low
EKF	[22, 39, 41]	Medium	High	High	Low
UKF	[23, 29]	High	V. High	High	High
PF	[47, 48]	V. High	High	V. High	High

According to Table 2, the LLKF shares the same merits as the EKF in terms of the low computational cost and dealing with slight nonlinearities, except for the slow response of the LLKF associated with a large initial state error. To depict the superiority of the EKF over the LLKF, the performance of both filters under different operating conditions is compared in Section V.

Assuming that the state vector is $[V_C \; SOC]^T$, the system output is V_t, the process noise is w, and the measurement noise is v, the discretized dynamics of the nonlinear system can be expressed in the following equations. Note that both w and v are vectors, independent, Gaussian, and having covariance matrices Q and R, respectively.

$$x_{k+1} = f(x_k, u_k) + w_k \tag{13}$$

$$y_k = g(x_k, u_k) + v_k \tag{14}$$

The EKF linearizes both state function and output function around the mean of the current state estimate ($\hat{x}$) using a first-order Taylor series. The Taylor expansion for (13) and (14) evaluated at the current state estimate ($\hat{x}$) can be expressed as:

$$x_{k+1} \approx f(\hat{x}_k, u_k) + A_k \left(x_k - \hat{x}_k\right) + w_k \tag{15}$$

$$y_k \approx g(\hat{x}_k, u_k) + C_k \left(x_k - \hat{x}_k\right) + v_k \tag{16}$$

where A_k and C_k are the partial derivatives (Jacobian matrices) of f (x_k, u_k) and g (x_k, u_k) with respect to x_k and evaluated at $\hat{x}_k$ as:

$$A_k = \left.\frac{\partial f(x_k, u_k)}{\partial x_k}\right|_{x_k=\hat{x}_k} \tag{17}$$

$$C_k = \left.\frac{\partial g(x_k, u_k)}{\partial x_k}\right|_{x_k=\hat{x}_k} \tag{18}$$

The EKF uses the system model along with the error between the measurement and the prediction to acquire the next state estimate. At each time step, the operation of the EKF can be summarized in two stages: initializing and updating. In the initializing stage, the state estimate and the estimation-error covariance of the previous time step can be attained as in (19) and (20), where the notation "$^-$" indicates that the variable is considered priorly. In the updating stage, the Kalman gain (K) is calculated in a way that minimizes P, and then it is applied to find the final state estimate and to update the current P as in (21)-(23) [22].

$$\hat{x}_k^- = f(\hat{x}_{k-1}, u_{k-1}) \tag{19}$$

$$P_k^- = A_{k-1} P_{k-1} A_{k-1}^T + Q \tag{20}$$

$$K_k = \frac{P_k^- C_k^T}{C_k P_k^- C_k^T + R} \tag{21}$$

$$\hat{x}_k = \hat{x}_k^- + K_k \left[y_k - g(\hat{x}_k^-, u_k) \right] \tag{22}$$

$$P_k = (I - K_k C_k) P_k^- \tag{23}$$

Fig. 5 clarifies the mechanism of Kalman gain to reduce the P in a loop structure. Note that R and Q are the only adjustable terms in the loop, and they play a vital role in the state convergence. Practically, R can be set based on multiple measures from the sensor after applying constant inputs from a precise power supply and taking out the mean values so that the noise covariance can be acquired. In the simulation scenario, R is set relatively small because only a slight sensor noise has been added. Q can be set intuitively; however, this may lead to filtering divergence over a long operation time, especially when R is set relatively small [33]. Therefore, in this paper, Q is set to be elected via a PSO algorithm from a preset searching range. PSO is a stochastic-based optimization algorithm that emulates the swarming and searching behavior of birds [50].

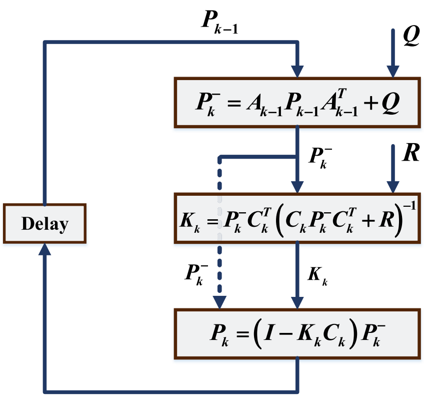

FIGURE 5. The dynamic mechanism of computing K_k and P_k of the EKF.

PSO has been used for a long time and been proven effective at searching for solutions in stochastic domains and finding optimums for both offline and online problems. PSO is initialized with a population of particles at random positions in the search space to look for the best position in the same space. The search space in our problem is supposed to have the best vector of the process noise covariance that satisfies the minimum state error covariance of the EKF for a comprehensive scenario of battery charging and discharging. The PSO is set to initialize with 50 random particles and to update particle positions at each iteration, where the iteration takes an undefined number of time samples. The PSO algorithm has to be applied offline because it requires a number of iterations to attain the optimal solution. Accordingly, the EKF has to execute once at each iteration. At each iteration, each particle updates its position and travels toward the best particle position (P_{best}) and the best global position (G_{best}). Thus, the next PSO iteration will be initialized based on the best positions. After completing the specified number of iterations, the vector of process noise covariance $[Q_1, Q_2]$ will be set to the final G_{best} vector. The performance evaluation is determined based on the fitness function, which uses the summation of absolute errors (SAE) formula. As the estimation-error covariance is a 2×2 matrix, the fitness function will only consider the diagonal terms in the matrix, as these are related to the main error not the mutual error of both states (V_C and SOC). The fitness function can be formed as a definite integration for the summation of the P diagonal terms, between the beginning time (t_1) and ending time (t_2) of an iteration, as:

$$fitness = \int_{t_1}^{t_2} |p_{11}| + |p_{22}| \tag{24}$$

The entire PSO operation to optimize the vector of the process noise covariance $[Q_1, Q_2]$ can be illustrated in the following steps:

Step1: Initialize random particles for the population
Step2: Evaluate the initial fitness for Q_1 and Q_2
Step3: Compare the evaluated fitness to the overall P_{best} to obtain the G_{best}
Step4: Save the P_{best} and the G_{best} at each iteration
Step5: Update repeatedly particle position and velocity according to P_{best} and G_{best}
Step6: Stop the algorithm after completing the specified number of iterations
Step7: Set the G_{best} vector to Q_1 and Q_2 of the EKF
Step8: End.

IV. MODEL PARAMETRIZATION AND SENSITIVITY ANALYSIS

The proposed battery model has five adjustable parameters—V_{OC}, R_0, R_1, R_{self}, and C—as shown in Fig. 1. Each parameter is supposed to be configured as a lookup table with four breakpoints for temperature (0°C, 15°C, 25°C, and 40°C) and nine breakpoints for SOC (0, 10, 25, 35, 50, 65, 75, 90, 100). The optimal parameters of the battery model have to be assigned via the parameterization process. The parameterization process is supposed to be repeated four times, according to the considered temperatures. First, a fully charged LiFePO4 lithium-ion battery is experimentally exposed to a pulse discharge current of 15 A under the four temperatures. Table 3 lists the manufacturing parameters of the utilized LiFePO4 lithium-ion battery. Considering the 25°C temperature as an example, the corresponding drop in the battery output voltage and the time-dependent recovery due to the discharge current is depicted in Fig. 6 in red. The parametrization process sets the optimal parameters for the battery model that can achieve a similar voltage profile to the experimental voltage profile when applying the same pulse current. Some studies have employed different

TABLE 3. Parameters of the utilized Lithium-ion.

Parameter	Value
Rated capacity	20 Ah
Rated voltage	3.3 V
Maximum manufacturing voltage	3.7 V
Maximum charging current	20 A
Discharge capability (continuous/transient)	20 A/100 A

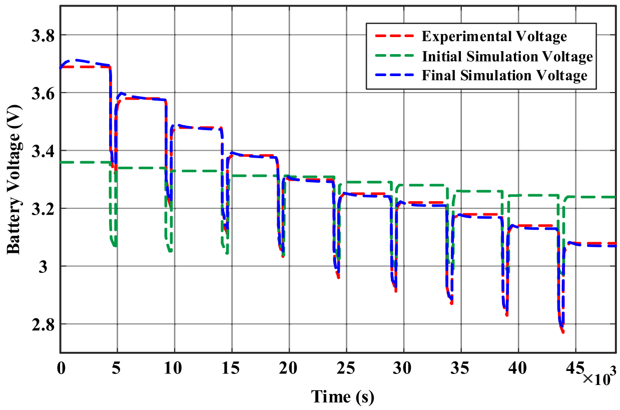

FIGURE 6. Voltage profiles during the parameterization process for the temperature of 25°C.

optimization methods, such as PSO and GA, to define the optimal parameters of a lithium-ion battery model [40], [41]. This study uses a ready library in MATLAB, known as the Simulink design optimization that utilizes multiple optimization algorithms to assign the optimal parameters of a model. Simulink design optimization requires a reference profile that is mostly derived from experimental data. The experimental voltage profile is imported into MATLAB/ Simulink and used as the reference profile.

By using the Simulink design optimization, the simulated model is run many times to reduce any mismatch between the simulated and experimental voltage profiles and find the optimal parameters of the model from a prespecified range. The initial and final voltage profiles are shown in Fig. 6 with green and blue colors, respectively. Table 4 (column: Reference values) lists a sample of the model optimal parameters for SOC = 50% at 25°C.

TABLE 4. Parameter sensitivity of battery model.

Parameter	Reference value	Variation range	Parameter sensitivity
R_0	0.0085	±25%	9.16 (V. high)
C	20300	±25%	6.45 (High)
R_1	0.0016	±25%	2.30 (Low)
R_{self}	83000	±25%	0.97 (V. low)

Second, a sensitivity analysis is conducted to investigate the effect of parameter variation on state estimation. Conducting a sensitivity analysis contributes in focusing on the key parameters during the tuning and preventing wasting time with the nonsensitive parameters. Also, assigning the sensitivity opens up prospects for finding correlations between sensitive parameters and external factors in the battery, such as battery capacity, thereby increasing the flexibility of the battery model to be used for different types or sizes of lithium-ion batteries. A common approach for sensitivity analysis, the one factor at a time (OFAT) method, is used. This approach tests the influence of varying each parameter individually when the other parameters remain fixed. The variation range comprises 21 cases, including a case for the reference value, ten above it, and ten below it. Therefore, the simulation is run 21 times for each of the four parameters. The variation step of each parameter is 2.5% of its reference value. The particular sensitivity (S_i) at each case can be derived in (25) when T_s is the number of time samples during the entire execution, and SOC_{ref} is the estimated SOC at the reference value of the parameter. The overall sensitivity of each parameter (S_P) can be defined in (26) with N equal to 21.

$$S_i = \frac{1}{Ts} \int \left| SOC_{ref} - SOC_i \right| \tag{25}$$

$$S_P = \sum_{i=1}^{N} S_i \tag{26}$$

Table 4 describes the final parameter sensitivity results at 25°C. The results denote a sensitivity gradient from very high to very low. V_{OC} primarily relies on SOC and does not have a tangible effect due to temperature change, so it is not counted in the sensitivity analysis. The initial internal resistor (R_0), followed by the hysteresis capacitor (C), exhibits the highest sensitivity among the parameters. Hence, the values of these two parameters attained in the parameterization process are depicted in Fig. 7 to show their reliance on variations of temperature and SOC. According to Fig. 7, R_0 has a high dependency and inverse proportionality to the temperature change. In contrast, C has relatively less dependence on temperature and more dependence on the SOC change. Nonetheless, both sensitive parameters need to be assigned carefully to ensure model accuracy.

Note that the sensitivity of the self-discharge resistor (R_{self}) is very low. Therefore, there is no need to design (R_{self}) as a lookup table since the slight change due to the variation of temperature or SOC will not affect the model accuracy.

V. RESULTS, DISCUSSION, AND LIMITATIONS

The original battery, the battery model, and the optimized EKF have been simulated in the Simulink and Simscape environments of MATLAB R2019b on an Intel core i7 CPU running 64-bit Windows 10 with 8 GB of RAM.

A. VERIFICATION RESULTS

Four major scenarios are considered to show the effectiveness of the proposed work.

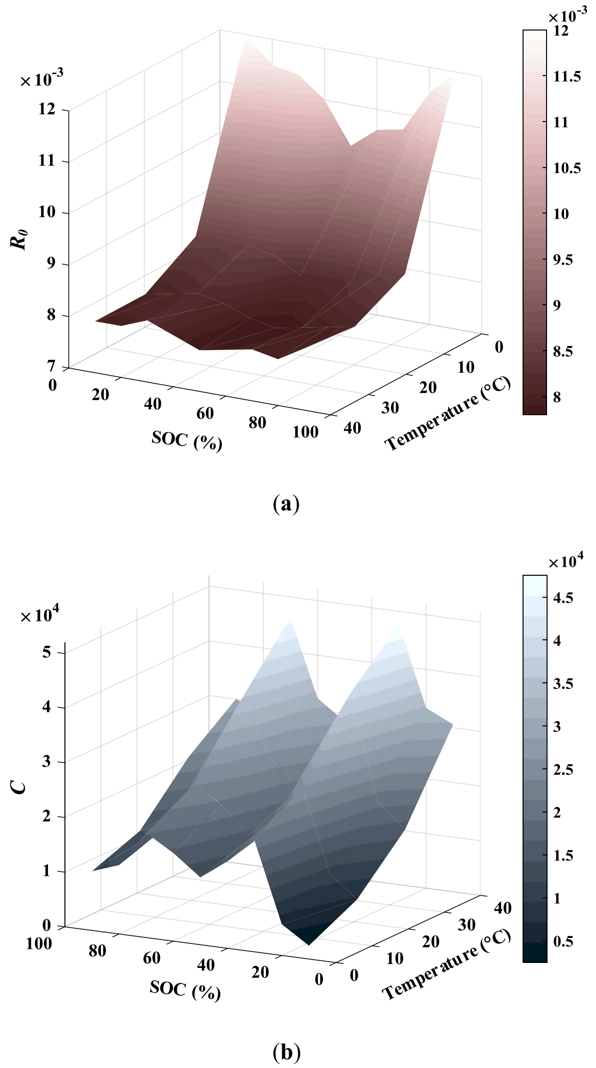

FIGURE 7. Parameter reliance on the variation of temperature and SOC: (a) Initial internal resistance (R_0), (b) Hysteresis capacitor (C).

1) SOC ESTIMATION WITH THE PROPOSED BATTERY MODEL

This case study presents a short-term SOC estimation using the proposed battery model. The battery model is applied to estimate the SOC using both the EKF and LLKF at temperatures of 0°C, 20°C, and 40°C. The LLKF approach applies the linear Kalman filter along with the battery model for SOC estimation. The SOC-V_{OC} relation can be represented as $V_{OC} = \lambda\ SOC + b$ [17]. To address the model nonlinearity, the LLKF approach considers only the slope (λ) in the SOC-V_{OC} relation changes online at each local point, while the intercept (b) is constant. Except for λ, which is multiplied by the SOC to map the V_{OC}, the state space matrices are derived normally from the dynamics of the battery model in (3)–(5). Two initial SOCs (50% and 100%) are considered for both the LLKF and EKF, whereas the actual initial SOC of the battery was 90%. The case study comprises discharging and charging scenarios between SOC = 90% and SOC = 30%. To emulate a realistic scenario in both charging and discharging modes, the discharging current is generated randomly for the range between 0.3 and 3 of the rated discharge current, whereas the charging current is assigned to be a typical MSCC current profile. Fig. 8 depicts the battery current under charging and discharging modes for the verification scenario.

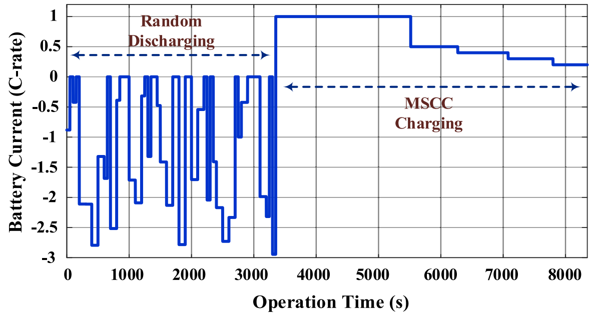

FIGURE 8. Charge-discharge current during verification scenarios.

Setting an initial SOC of 50%, the results identify a significant estimation error at the beginning when using the LLKF, as shown in Figs. 9, 10, and 11.

Additionally, the LLKF requires more execution time to compensate the error and reach the original SOC because its procedure comprises two phases of linearization and estimation at each breaking interval. Although the error is reduced by reducing the initial SOC error, a large initial SOC error can be expected in any real scenario. By using the EKF with the proposed method of capacity estimation, the average estimation error under all temperatures is minimized by approximately 6.4% when the initial SOC is 50% and by approximately 1.9% when the initial SOC is 100%. Moreover, by running each approach individually, the simulation of the EKF with the proposed battery model and capacity estimation method requires less execution time compared to the execution time needed for the LLKF (see Figs 9-d, 9-f, 10-d, 10-f, 11-d, and 11-f). This means that the computational cost of the proposed approach is more acceptable than that of the LLKF.

2) BATTERY CAPACITY ESTIMATION

The proposed estimation technique of battery capacity degradation is applied and compared to the method of using an extra Kalman filter to track the actual capacity [29], [30]. The extra Kalman filter is used to eliminate the measurement noise and estimate the actual capacity from the measured capacity via the Coulomb counting approach when both initial and final SOCs for all cycles are known. Two aging conditions are considered: 90% and 100% of the initial capacity. The comparison comprises 18 charge-discharge cycles. Along with the obvious simplicity, the proposed technique shows its effectiveness in estimating the current capacity of the battery accurately. The absolute error between the capacity values estimated by both methods is shown in Figs. 12-c and 12-d. Considering the 100% aging condition, the error between the real capacity and the estimated

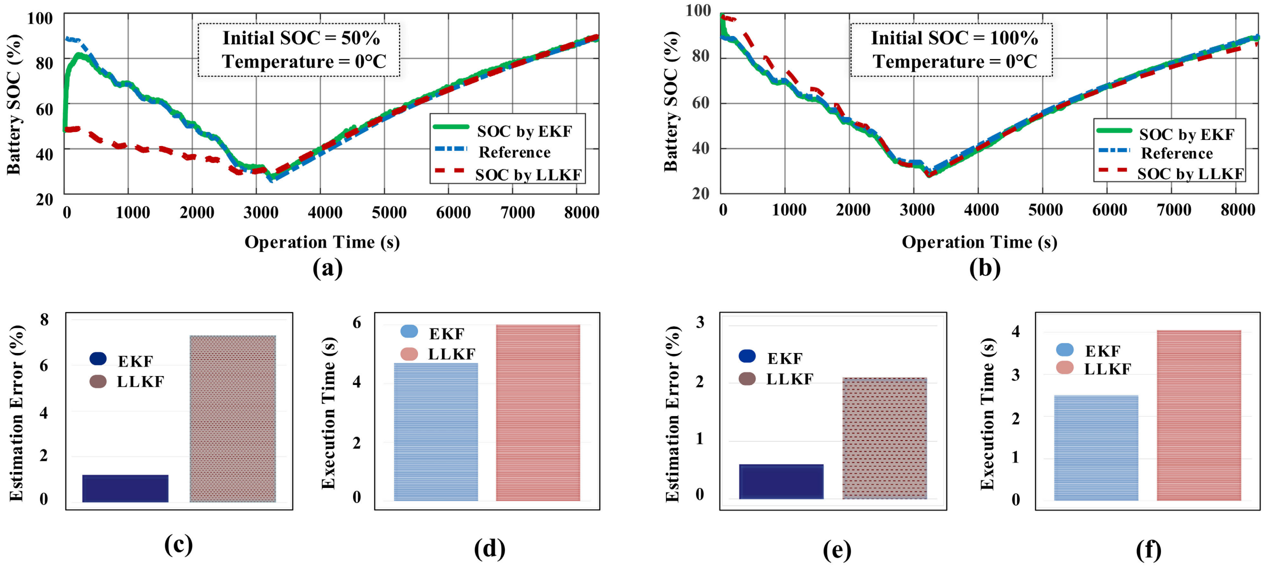

FIGURE 9. SOC estimation for the proposed model via EKF and LLKF for temperature = 0°C: (a) One-cycle SOC for initial SOC = 50%; (b) One-cycle SOC for initial SOC = 100%, (c) Average estimation error for initial SOC = 50%, (d) Simulink execution time for initial SOC = 50%, (e) Average estimation error for initial SOC = 100%, (f) Simulink execution time for initial SOC = 100%.

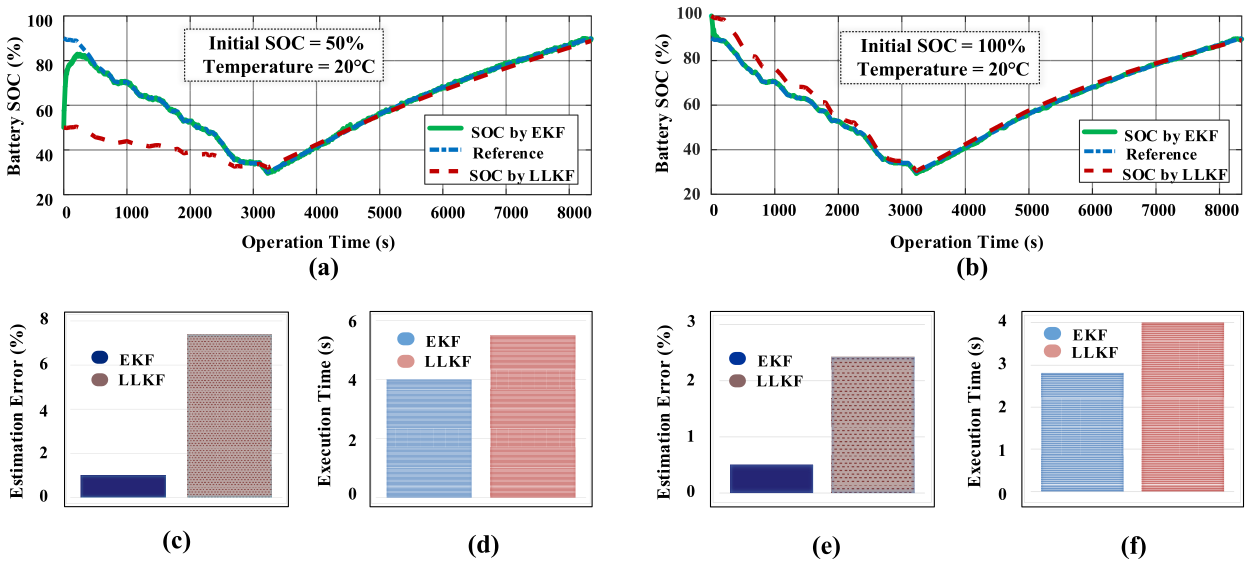

FIGURE 10. SOC estimation for the proposed model via EKF and LLKF for temperature = 20°C: (a) One-cycle SOC for initial SOC = 50%, (b) One-cycle SOC for initial SOC = 100%, (c) Average estimation error for initial SOC = 50%, (d) Simulink execution time for initial SOC = 50%, (e) Average estimation error for initial SOC = 100%, (f) Simulink execution time for initial SOC = 100%.

capacity is mitigated with the proposed approach. According to Fig. 12-e, the average absolute error of the capacity estimation during 18 cycles is reduced to half compared to the method using the extra Kalman filter. Considering the 90% aging condition, Fig. 12-g reflects an increment in the average absolute error via the proposed method, which primarily relates to the first cycle. The reason behind this error increment comes from setting the new capacity at the end of the charging mode in the proposed approach. In contrast, this is set at the end of discharging mode in the approach using the extra Kalman filter. By running each approach individually and considering only the first cycle, the execution time of the proposed estimation technique of battery capacity is reduced by approximately 1.25s compared to the method using the extra Kalman filter during both aging conditions (see Fig. 12-f and Fig. 12-h). This corroborates that the implementation of the proposed approach requires comparatively less processing resources (time and memory).

3) OUTPUT VOLTAGE ESTIMATION ERROR

In this subsection, a comparison between the measured output voltage and the estimated output voltage via the optimized EKF is conducted and shown in Fig. 13. The effective estimation of the optimized EKF and the proposed model can

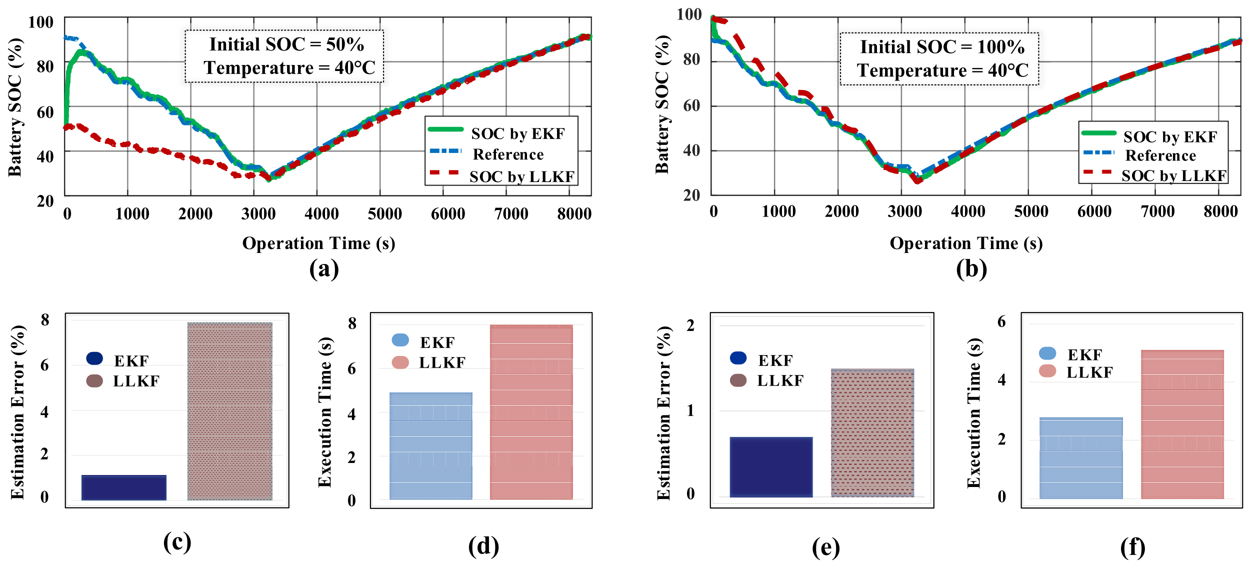

FIGURE 11. SOC estimation for the proposed model via EKF and LLKF for temperature = 40°C: (a) One-cycle SOC for initial SOC = 50%, (b) One-cycle SOC for initial SOC = 100%, (c) Average estimation error for initial SOC = 50%, (d) Simulink execution time for initial SOC = 50%, (e) Average estimation error for initial SOC = 100%, (f) Simulink execution time for initial SOC = 100%.

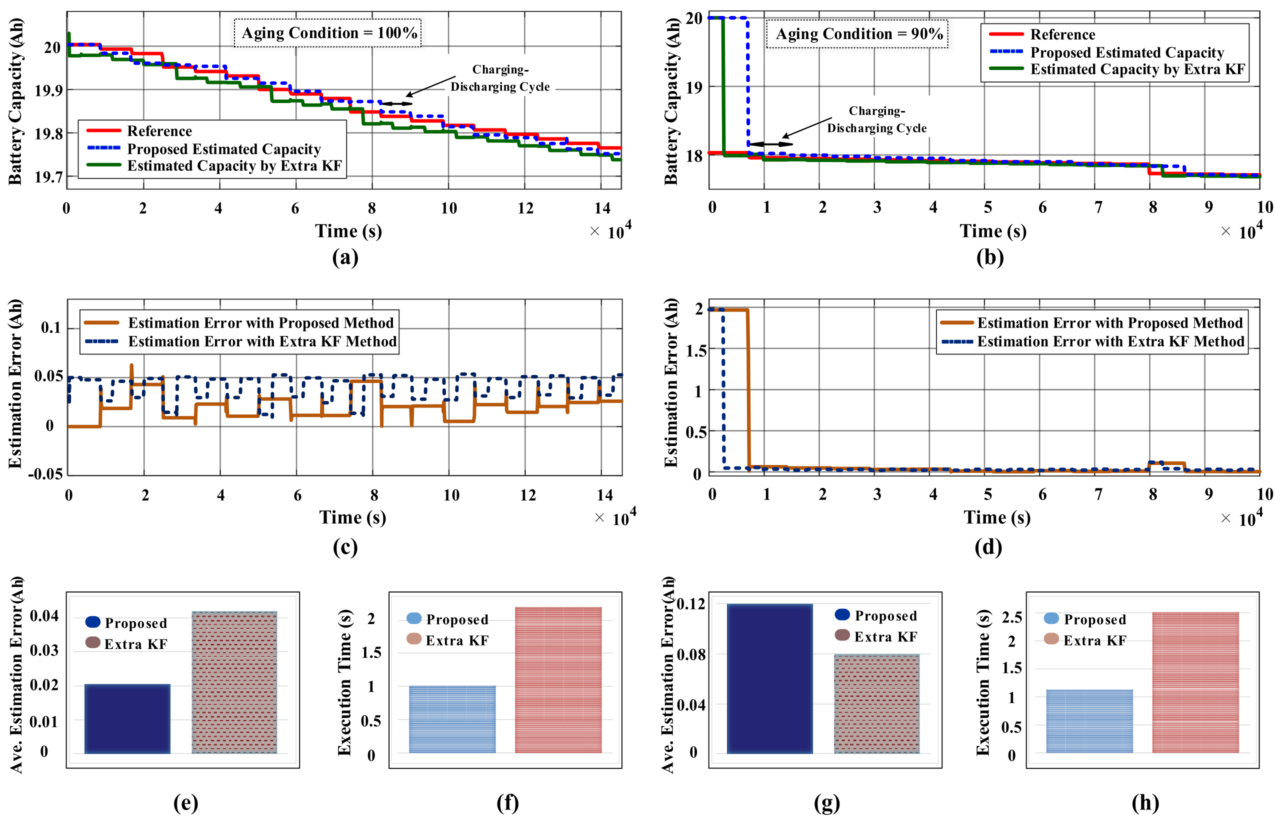

FIGURE 12. Capacity estimation by the proposed method and the method using extra Kalman filter: (a) Capacity via both methods for 100% aging condition, (b) Capacity via both methods for 90% aging condition, (c) Absolute estimation error for 100% aging condition, (d) Absolute estimation error for 90% aging condition, (e) Average estimation error during 18 cycles for 100% aging condition, (f) Execution time for the first cycle considering 100% aging condition, (g) Average estimation error during 12 cycles for 90% aging condition, (h) Execution time for the first cycle considering 90% aging condition.

be measured through the capability of matching both output voltages and minimizing the voltage-estimation error towards zero. Fig. 13-b demonstrates the voltage estimation error that increases during the discharging mode due to the irregular discharge current. Even with the irregular discharge current, the voltage estimation error lies between -0.1 V and 0.09 V

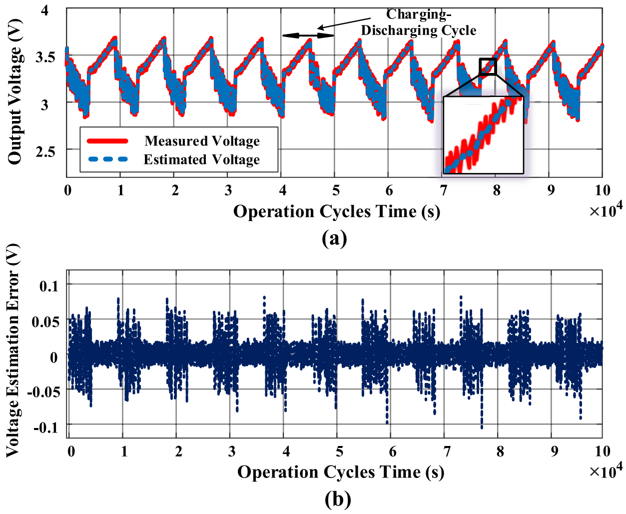

FIGURE 13. **Verifying the output voltage estimation: (a) Measured voltage and estimated voltage via the EKF, (b) Voltage estimation error.**

in the worst cases. Therefore, an estimation divergence is not expected to occur during different operating conditions.

4) SOC ESTIMATION VIA EKF WITH UTILIZING PSO ALGORITHM

The reference SOC of the battery is acquired by using the Coulomb counting method with the accurate values for both initial SOC and capacity degradation rate, and compared with the estimated SOC via the EKF along with the proposed battery model. The comparison includes 12 repeated charge-discharge cycles, as shown in Fig. 14-a. Fig. 14-b depicts a slight estimation error for the SOC, within 0.7%, which verifies the excellent performance of the entire system (EKF and battery model). However, this estimation error

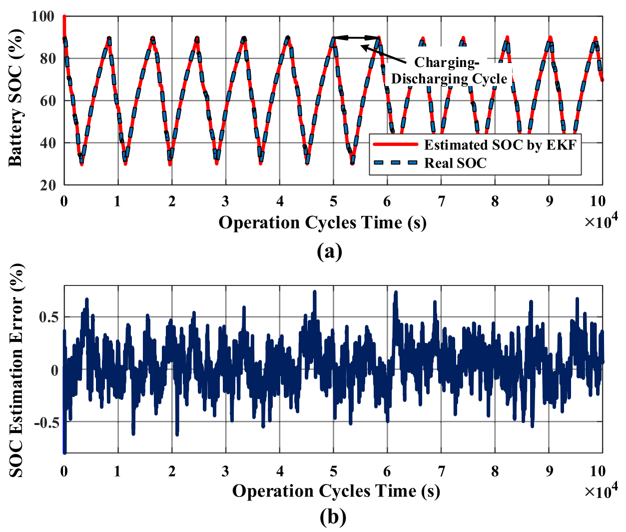

FIGURE 14. **Verifying the long-term SOC estimation: (a) Estimated SOC by the optimized EKF and the real SOC, (b) SOC estimation error.**

was acquired when using the optimal vector of the process noise covariance $[Q_1, Q_2]$ after completing 60 iterations. The PSO algorithm was applied offline to optimize the vector of the process noise covariance, and it was initialized with 50 random particles in the searching space. The algorithm required less than 30 minutes to reach the optimal vector of the process noise covariance. Fig. 15-a and Fig. 15-b show the optimal values of the process noise covariance Q_1 and Q_2 at each iteration, respectively.

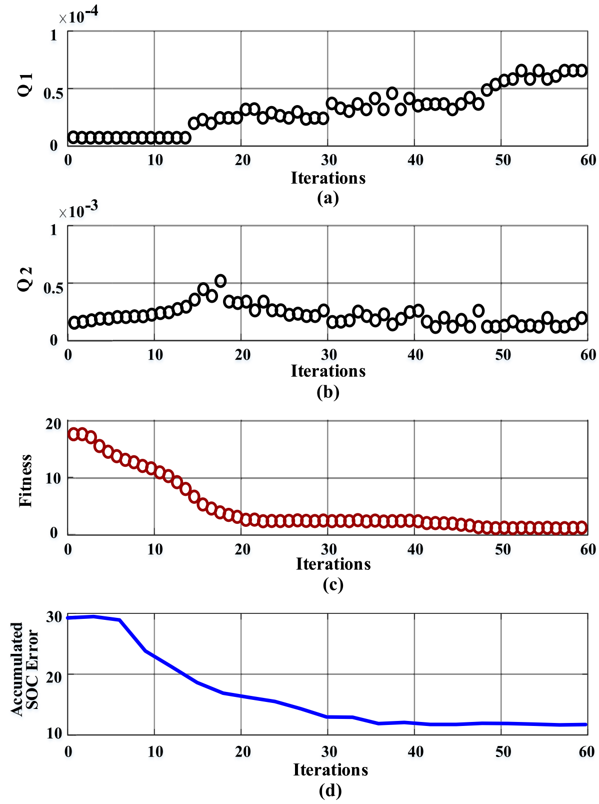

FIGURE 15. **Application of PSO Algorithm to Optimize Q_1 and Q_2: (a) Optimal values of Q_1 at each iteration, (b) Optimal values of Q_2 at each iteration, (c) The fitness function development, (d) The accumulated absolute error of SOC at each iteration.**

Fig. 15-c shows the development of the fitness function at each iteration, which clarifies the gradual decrement of P. Finally, Fig. 15-d illustrates the accumulated absolute error of the SOC during the entire time of iterations. Giving that the algorithm is initialized with a random vector of the process noise covariance, the fitness function, which comprises the vector of the accumulated absolute error covariance, was minimized to the lowest possible vector. Moreover, the accumulated SOC error at the last iteration was reduced by almost 20% compared to the first iteration.

B. PERFORMANCE DISCUSSION

1) ESTIMATION ACCURACY

According to Figs. 9, 10, and 11, the SOC estimation error for the proposed combination of the battery model and the optimized EKF lies between 0.5% and 1.25% for all tested temperatures. This verifies that the proposed model has enabled its state estimator to capture the dynamics of the real battery even when essential parameters change due to altered temperature. This is crucial because without careful handling of the temperature effect, the temperature change can influence the internal resistance directly and thereby affect the model accuracy. In addition to the estimation accuracy, the optimized EKF ensures a fast response for state updating when starting with a significant initial error. The reason behind the fast convergence is that the optimized EKF uses a ready-made system in which its dynamics are linearized at each time sample. Hence, the state update changes correspondingly at each time sample. Whereas the LLKF uses a piecewise or another linearization approach, the model trajectory itself is divided into several linear pieces priorly. The slow convergence when starting with a significant error in the initial state occurs due to the inability of the Kalman gain to compensate for the error, especially at the end of each piece or interval. Moreover, the results of the optimization process depict two facts. The first fact is that the slight change in the vector of estimation error covariance away from its optimal values can significantly affect the estimation accuracy. Therefore, such optimization is necessary to assign the P vector for each particular sensor with a specific R. The second fact is that the suggested fitness function has a strong correlation and direct proportion with the accumulated estimation error. Thus, the fitness function can ensure reaching the lowest possible estimation error for the given parameters.

2) COMPUTATIONAL COMPLEXITY

Improvements in estimation algorithms for battery states should avoid increasing the computational burden or even reduce it. The SOC estimation approach is compared to the LLKF approach, which shares many attributes with the EKF, especially considering the computational burden, as shown in Table 2. This shared property is verified via the results, which can also be elucidated by considering the complexity order of both approaches. The EKF has almost the same typical complexity as the basic Kalman filter, which is $O(\mathrm{n}^{2.376})$ [51]. Nonetheless, additional complexity may come from the observation equations and process update. The complexity of the linearized process update is $O(\mathrm{n})$, while the complexity of the observation function is nearly constant [51]. The additional complexity for the EKF with discounting the complexity of the Kalman filter can be defined as max ($O(\mathrm{n})$, $O(1)$), which is $O(\mathrm{n})$. For the LLKF, the complexity of piecewise linearization should be taken into account. Thus, the additional complexity for using the LLKF with discounting the complexity of the Kalman filter is no less than $O(\mathrm{mn})$, where m is the breakpoints of the pieces [52]. The number of breakpoints needs to be assigned carefully to maintain reasonable performance by balancing between accuracy and complexity. Figs. 9, 10, and 11 interpret this tradeoff between accuracy and computational complexity of the LLKF in which the number of breakpoints is suitable for a small initial error. For a significant initial error, the number of breakpoints should be increased, which will increase the processing time as well. Based on Figs. 9-d, 9-f, 10-d, 10-f, 11-d, and 11-f, the use of the optimized EKF reduces the execution time for all temperatures by approximately 2 s on average when the initial SOC is 50% and by approximately 1.3 s on average when the initial SOC is 100% compared to the use of the LLKF. For the entire system, the computational complexity is minimized via both the state observer and the battery model structure, including the capacity model. The utilized RC model requires the lowest computational complexity in terms of model structure. For the capacity assessment, replacing the linear model and the Kalman filter by a comparator and PI compensator interprets reducing the execution time by approximately 1.25 s for 100% initial aging and by approximately 1.4 s for 90% initial aging, as shown in Fig. 12.

C. STUDY LIMITATIONS

This study encountered some limitations that can be addressed in the future:

1) The experimental data are achieved for a specific type of lithium-ion battery (*i.e.,* LiFePO4). More types may be examined to generalize the approach further.
2) The self-discharge resistance (R_{self}), which is set during the overall parametrization procedure, needs to be more specified and parameterized individually through a time-consuming procedure to obtain the precise value.

VI. CONCLUSION

This paper proposed an enhanced model for lithium-ion batteries used in the precise estimation of battery SOC and capacity. The proposed model involved several factors, such as addressing the issue of nonlinearity introduced by the influence of the operating temperature and adopting a simple technique to emulate the aging process. The use of the EKF is verified to be the perfect choice for the SOC estimation of lithium-ion batteries since it copes with the slight nonlinearity of SOC-V_{SOC} and requires less computational cost compared to other linear and nonlinear versions of the Kalman filter. This paper proposed a modification in the use of the EKF that exploits the PSO algorithm to optimize the vector of process noise covariance and avoid any estimation divergence that may occur due to accumulated errors during longtime operation. The performance of the proposed approach for SOC estimation is verified under different temperatures and compared to the LLKF approach. The simulation results have shown significant enhancement in state estimation compared to the LLKF, especially for large errors in the initial SOC. Concerning the degraded capacity estimation, the proposed approach has shown its effectiveness for different aging conditions. The proposed approach was also verified to be computationally efficient compared to the method that uses an additional Kalman filter for capacity estimation.

REFERENCES

[1] A. B. Khan and W. Choi, ''Optimal charge pattern for the high-performance multistage constant current charge method for the Li-ion batteries,'' *IEEE Trans. Energy Convers.*, vol. 33, no. 3, pp. 1132–1140, Sep. 2018.

[2] Y. Xing, W. He, M. Pecht, and K. L. Tsui, ''State of charge estimation of lithium-ion batteries using the open-circuit voltage at various ambient temperatures,'' *Appl. Energy*, vol. 113, pp. 106–115, Jan. 2014.

[3] L. Lavigne, J. Sabatier, J. M. Francisco, F. Guillemard, and A. Noury, ''Lithium-ion open circuit voltage (OCV) curve modelling and its ageing adjustment,'' *J. Power Sources*, vol. 324, pp. 694–703, Aug. 2016.

[4] X. Dang, L. Yan, H. Jiang, X. Wu, and H. Sun, ''Open-circuit voltage-based state of charge estimation of lithium-ion power battery by combining controlled auto-regressive and moving average modeling with feedforward-feedback compensation method,'' *Int. J. Electr. Power Energy Syst.*, vol. 90, pp. 27–36, Sep. 2017.

[5] Y. Song, M. Park, M. Seo, and S. W. Kim, ''Improved SOC estimation of lithium-ion batteries with novel SOC-OCV curve estimation method using equivalent circuit model,'' in *Proc. 4th Int. Conf. Smart Sustain. Technol. (SpliTech)*, Jun. 2019, pp. 1–6.

[6] G. S. Misyris, D. I. Doukas, T. A. Papadopoulos, D. P. Labridis, and V. G. Agelidis, ''State-of-charge estimation for Li-ion batteries: A more accurate hybrid approach,'' *IEEE Trans. Energy Convers.*, vol. 34, no. 1, pp. 109–119, Mar. 2019.

[7] J. Xie, J. Ma, and K. Bai, ''Enhanced Coulomb counting method for state-of-charge estimation of lithium-ion batteries based on Peukert's law and Coulombic efficiency,'' *J. Power Electron.*, vol. 18, no. 3, pp. 910–922, 2018.

[8] L. Zhao, M. Lin, and Y. Chen, ''Least-squares based Coulomb counting method and its application for state-of-charge (SOC) estimation in electric vehicles,'' *Int. J. Energy Res.*, vol. 40, no. 10, pp. 1389–1399, Aug. 2016.

[9] J. Meng, M. Ricco, G. Luo, M. Swierczynski, D.-I. Stroe, A.-I. Stroe, and R. Teodorescu, ''An overview and comparison of online implementable SOC estimation methods for lithium-ion battery,'' *IEEE Trans. Ind. Appl.*, vol. 54, no. 2, pp. 1583–1591, Mar. 2018.

[10] J. Rivera-Barrera, N. Muñoz-Galeano, and H. Sarmiento-Maldonado, ''SoC estimation for lithium-ion batteries: Review and future challenges,'' *Electronics*, vol. 6, no. 4, p. 102, Nov. 2017.

[11] M. A. Varnosfaderani and D. Strickland, ''Online impedance spectroscopy estimation of a battery,'' in *Proc. 18th Eur. Conf. Power Electron. Appl. (EPE ECCE Europe)*, Sep. 2016, pp. 1–10.

[12] J. A. A. Qahouq and Z. Xia, ''Single-Perturbation-Cycle online battery impedance spectrum measurement method with closed-loop control of power converter,'' *IEEE Trans. Ind. Electron.*, vol. 64, no. 9, pp. 7019–7029, Sep. 2017.

[13] J. Chen, Q. Ouyang, C. Xu, and H. Su, ''Neural network-based state of charge observer design for lithium-ion batteries,'' *IEEE Trans. Control Syst. Technol.*, vol. 26, no. 1, pp. 313–320, Jan. 2018.

[14] J. Wu, C. Zhang, and Z. Chen, ''An online method for lithium-ion battery remaining useful life estimation using importance sampling and neural networks,'' *Appl. Energy*, vol. 173, pp. 134–140, Jul. 2016.

[15] T. Zahid, K. Xu, W. Li, C. Li, and H. Li, ''State of charge estimation for electric vehicle power battery using advanced machine learning algorithm under diversified drive cycles,'' *Energy*, vol. 162, pp. 871–882, Nov. 2018.

[16] M. Ali, M. Kamran, P. Kumar, S. Nengroo, M. Khan, A. Hussain, and H.-J. Kim, ''An online data-driven model identification and adaptive state of charge estimation approach for lithium-ion-batteries using the Lagrange multiplier method,'' *Energies*, vol. 11, no. 11, p. 2940, Oct. 2018.

[17] W. Wang and J. Mu, ''State of charge estimation for lithium-ion battery in electric vehicle based on Kalman filter considering model error,'' *IEEE Access*, vol. 7, pp. 29223–29235, 2019.

[18] Z. Yu, R. Huai, and L. Xiao, ''State-of-charge estimation for lithium-ion batteries using a Kalman filter based on local linearization,'' *Energies*, vol. 8, no. 8, pp. 7854–7873, Jul. 2015.

[19] P. Shrivastava, T. K. Soon, M. Y. I. B. Idris, and S. Mekhilef, ''Overview of model-based online state-of-charge estimation using Kalman filter family for lithium-ion batteries,'' *Renew. Sustain. Energy Rev.*, vol. 113, Oct. 2019, Art. no. 109233.

[20] J. Xu, C. C. Mi, B. Cao, J. Deng, Z. Chen, and S. Li, ''The state of charge estimation of lithium-ion batteries based on a proportional-integral observer,'' *IEEE Trans. Veh. Technol.*, vol. 63, no. 4, pp. 1614–1621, May 2014.

[21] U. Amir, L. Tao, X. Zhang, M. Saeed, and M. Hussain, ''A novel SOC estimation method for lithium ion battery based on improved adaptive PI observer,'' in *Proc. IEEE Int. Conf. Electr. Syst. for Aircr., Railway, Ship Propuls. Road Vehicles Int. Transp. Electrific. Conf. (ESARS-ITEC)*, Nov. 2018, pp. 1–5.

[22] Y. Ma, P. Duan, P. He, F. Zhang, and H. Chen, ''FPGA implementation of extended Kalman filter for SOC estimation of lithium-ion battery in electric vehicle,'' *Asian J. Control*, vol. 21, no. 4, pp. 2126–2136, Jul. 2019.

[23] W. Wang, X. Wang, C. Xiang, C. Wei, and Y. Zhao, ''Unscented Kalman filter-based battery SOC estimation and peak power prediction method for power distribution of hybrid electric vehicles,'' *IEEE Access*, vol. 6, pp. 35957–35965, 2018.

[24] Y. Song, D. Liu, Y. Hou, J. Yu, and Y. Peng, ''Satellite lithium-ion battery remaining useful life estimation with an iterative updated RVM fused with the KF algorithm,'' *Chin. J. Aeronaut.*, vol. 31, no. 1, pp. 31–40, Jan. 2018.

[25] E. Brun, ''Key performance indicators for the monitoring of large-scale battery storage systems,'' M.S. thesis, KTH School Ind. Eng. Manage. Energy Technol., Stockholm, Sweden, 2019.

[26] Y. Li, M. Abdel-Monem, R. Gopalakrishnan, M. Berecibar, E. Nanini-Maury, N. Omar, P. van den Bossche, and J. Van Mierlo, ''A quick on-line state of health estimation method for Li-ion battery with incremental capacity curves processed by Gaussian filter,'' *J. Power Sources*, vol. 373, pp. 40–53, Jan. 2018.

[27] C. She, Z. Wang, F. Sun, P. Liu, and L. Zhang, ''Battery aging assessment for real-world electric buses based on incremental capacity analysis and radial basis function neural network,'' *IEEE Trans. Ind. Informat.*, vol. 16, no. 5, pp. 3345–3354, May 2020.

[28] Z. Wang, J. Ma, L. Zhang, ''State-of-health estimation for lithium-ion batteries based on the multi-island genetic algorithm and the Gaussian process regression,'' *IEEE Access*, vol. 5, pp. 21286–21295, Oct. 2017.

[29] I. Nagi, D. Yin, A. Yousafzai, D. Tzannetos, O. J. Mengshoel, R. Martin, and C. S. Kulkarni, ''Exploring Gaussian process regression and unscented Kalman filtering for lithium-ion battery prognostics,'' in *Proc. AIAA Scitech Forum*, 2019, p. 0685.

[30] S. Li, S. Pischinger, C. He, L. Liang, and M. Stapelbroek, ''A comparative study of model-based capacity estimation algorithms in dual estimation frameworks for lithium-ion batteries under an accelerated aging test,'' *Appl. Energy*, vol. 212, pp. 1522–1536, Feb. 2018.

[31] L. Chen, Z. Lü, W. Lin, J. Li, and H. Pan, ''A new state-of-health estimation method for lithium-ion batteries through the intrinsic relationship between ohmic internal resistance and capacity,'' *Measurement*, vol. 116, pp. 586–595, Feb. 2018.

[32] S. Wang, Y. Yang, and K. Guo, ''An improved recursive total least squares estimation of capacity for electric vehicle lithium-iron phosphate batteries,'' *Math. Problems Eng.*, vol. 2020, pp. 1–12, Jun. 2020.

[33] S. Fakoorian, A. Mohammadi, V. Azimi, and D. Simon, ''Robust Kalman-type filter for non-Gaussian noise: Performance analysis with unknown noise covariances,'' *J. Dyn. Syst., Meas., Control*, vol. 141, no. 9, pp. 1–9, Sep. 2019.

[34] A. Medjghou, M. Ghanai, and K. Chafaa, ''A robust feedback linearization control framework using an optimized extended Kalman filter,'' *J. Eng. Sci. Technol. Rev.*, vol. 10, no. 5, pp. 1–8, 2017.

[35] A. S. Tummala, M. R. Chintala, and R. Pilla, ''Tuning of extended Kalman filter using self-adaptive differential evolution algorithm for sensorless permanent magnet synchronous motor drive,'' *Int. J. Eng.*, vol. 29, no. 11, pp. 1565–1573, 2016.

[36] A. Medjghou, M. Ghanai, and K. Chafaa, ''BBO optimization of an EKF for interval type-2 fuzzy sliding mode control,'' *Int. J. Comput. Intell. Syst.*, vol. 11, no. 1, pp. 770–789, 2018.

[37] Z. Beheshti and S. M. H. Shamsuddin, ''A review of population-based meta-heuristic algorithms,'' *Int. J. Adv. Soft Comput. Appl*, vol. 5, no. 1, pp. 1–35, 2013.

[38] N. Chen, P. Zhang, J. Dai, and W. Gui, ''Estimating the state-of-charge of lithium-ion battery using an H-infinity observer based on electrochemical impedance model,'' *IEEE Access*, vol. 8, pp. 26872–26884, 2020.

[39] Y. Chen, Y. Ma, P. Duan, and H. Chen, ''Estimation of state of charge for lithium-ion battery considering effect of aging and temperature,'' in *Proc. 37th Chin. Control Conf. (CCC)*, Jul. 2018, pp. 8472–8477.

[40] M. Hu, Y. Li, S. Li, C. Fu, D. Qin, and Z. Li, ''Lithium-ion battery modeling and parameter identification based on fractional theory,'' *Energy*, vol. 165, pp. 153–163, Dec. 2018.

[41] Y. Zheng, W. Gao, M. Ouyang, L. Lu, L. Zhou, and X. Han, ''State-of-charge inconsistency estimation of lithium-ion battery pack using mean-difference model and extended Kalman filter,'' *J. Power Sources*, vol. 383, pp. 50–58, Apr. 2018.

[42] Y. Tang, T. Li, and X. Cheng, ''Review of specific heat capacity determination of lithium-ion battery,'' *Energy Procedia*, vol. 158, pp. 4967–4973, Feb. 2019.

[43] L. Jiang, Y. Li, Y. Huang, J. Yu, X. Qiao, Y. Wang, C. Huang, and Y. Cao, ''Optimization of multi-stage constant current charging pattern based on Taguchi method for Li-ion battery,'' *Appl. Energy*, vol. 259, Feb. 2020, Art. no. 114148.

[44] R. P. Ramasamy, R. E. White, and B. N. Popov, ''Calendar life performance of pouch lithium-ion cells,'' *J. Power Sources*, vol. 141, no. 2, pp. 298–306, Mar. 2005.

[45] T. O. Ting, K. L. Man, E. G. Lim, and M. Leach, ''Tuning of Kalman filter parameters via genetic algorithm for state-of-charge estimation in battery management system,'' *Sci. World J.*, vol. 2014, pp. 1–11, Aug. 2014.

[46] M. Mastali, J. Vazquez-Arenas, R. Fraser, M. Fowler, S. Afshar, and M. Stevens, ''Battery state of the charge estimation using Kalman filtering,'' *J. Power Sources*, vol. 239, pp. 294–307, Oct. 2013.

[47] L. Zheng, J. Zhu, G. Wang, D. D.-C. Lu, and T. He, ''Differential voltage analysis based state of charge estimation methods for lithium-ion batteries using extended Kalman filter and particle filter,'' *Energy*, vol. 158, pp. 1028–1037, Sep. 2018.

[48] T.-T. Nguyen, A. B. Khan, Y. Ko, and W. Choi, ''An accurate state of charge estimation method for lithium iron phosphate battery using a combination of an unscented Kalman filter and a particle filter,'' *Energies*, vol. 13, no. 17, p. 4536, Sep. 2020.

[49] S. Biswas, ''Computationally efficient non-linear Kalman filters for on-board space vehicle navigation,'' Ph.D. dissertation, School Elect. Eng. Telecommun., Univ. New South Wales, Sydney, NSW, Australia, 2017.

[50] M. A. Hossain, H. R. Pota, S. Squartini, and A. F. Abdou, ''Modified PSO algorithm for real-time energy management in grid-connected microgrids,'' *Renew. Energy*, vol. 136, pp. 746–757, Jun. 2019.

[51] C. Montella. (2011). *The Kalman Filter and Related Algorithms: A Literature Review*. [Online]. Available: https://www.researchgate.net/publication/236897001_The_Kalman_Filter_and_Related_Algorithms_A_Literature_Review

[52] M. Rewienski and J. White, ''A trajectory piecewise-linear approach to model order reduction and fast simulation of nonlinear circuits and micromachined devices,'' *IEEE Trans. Comput.-Aided Design Integr. Circuits Syst.*, vol. 22, no. 2, pp. 155–170, Feb. 2003.

RASOOL M. IMRAN received the B.Sc. degree in electrical engineering from Al-Furat Al-Awsat Technical University, Iraq, in 2011, the M.Tech. degree from the Sam Higginbottom Institute of Agriculture, Technology and Sciences, India, in 2014, and the Ph.D. degree from the Huazhong University of Science and Technology, China, in 2018. He is currently an Assistant Professor with the School of Artificial Intelligence, Wuchang University of Technology, China. His research interests include microgrid control and stability, management of renewable energy sources, battery management systems, and predictive control of electric vehicles.

QIANG LI received the B.Sc. degree in car design from the Henan University of Science and Technology, Luoyang, China, in 1999, the M.S. degree in mechatronic engineering from Northwestern Polytechnic University, Xi'an, China, in 2007, and the Ph.D. degree in mechanical engineering from Tsinghua University, Beijing, China, in 2013. He is currently an Associate Professor with the School of Artificial Intelligence, Wuchang University of Technology, Wuhan, China. His research interests include vibration isolators and structural dynamics.

FIRAS M. F. FLAIH (Member, IEEE) received the B.Sc. degree in electrical engineering from Mosul University, Iraq, in 2005, the M.Tech. degree in electrical and electronics engineering from the Sam Higginbottom Institute of Agriculture, Technology and Sciences, India, in 2014, and the Ph.D. degree in electrical engineering from the Huazhong University of Science and Technology, China, in 2017. He is currently a Chief Engineer with the State Company of the North Distribution Electricity, Ministry of Electricity, Iraq. His research interests include distribution networks, distributed generators, and smart grids. He is also a reviewer of many respected journals, including the IEEE TRANSACTIONS ON SMART GRID, the IEEE TRANSACTIONS ON POWER SYSTEM, IEEE ACCESS, and the *International Journal of Numerical Modelling: Electronic Networks, Devices and Fields*.